Multiscale solidification simulation of Sr-modified Al-Si-Mg alloy in die casting

IOP Conf. Series: Materials Science and Engineering **861** (2020) 012034 doi:10.1088/1757-899X/861/1/012034

Multiscale solidification simulation of Sr-modified Al-Si-Mg alloy in die casting

B Zhou, G Laschet, J Eiken, H Behnken and M Apel

Access e.V., Intzestr. 5, 52072 Aachen, Germany

Email: b.zhou@access-technology.de

Abstract. Thermomechanical casting simulations incorporating solidification models are widely applied to improve the dimensional accuracy of casting components. The solidification path is commonly described based on Scheil-Gulliver assumptions which however fail to describe the effect of Strontium in Sr-modified Al-Si-Mg casting alloys. Strontium, even in small amounts, strongly affects the solidification morphology of the Al-Si eutectic together with its growth undercooling and hence the fraction solid–temperature relation during later stages of solidification. In order to address this problem, a dedicated micro-macro simulation approach is proposed here. The macroscopic thermomechanical casting simulation is linked with a spatially resolved multi-phase field simulation of the microstructure. Due to the fine fibrous morphology of the Si eutectic, a two-level homogenization scheme was applied to derive the effective mechanical properties of the Al alloy during its solidification. The proposed multiscale simulation and homogenization approach was applied to a permanent mould casting using an axisymmetric bowl cast from A356 for experimental validation.

1. Introduction

Al-Si based alloys are widely applied for light weight components due to their excellent castability, low weight, corrosion resistance and good strength. In commercial applications, additional chemical modifiers are added to the Al-Si alloys to modify the Al-Si eutectic in order to improve mechanical properties. Strontium (Sr) addition in range between 100ppm and 400ppm transforms the eutectic morphology from coarse plate-like structure to a fine coral-like fibrous networks [1, 2]. This finer and homogenous eutectic morphology strongly improves the ductility of the casting alloy and reduces the possibility of crack formation [3].

The mechanism of Sr-modification to the eutectic solidification has been well studied by several experimental works. Sr impacts both growth and nucleation of the eutectic Si phase. Lu and Hellawell [4] found that the absorbed Sr atoms at the interface hinder the growth of Si phase in twin-plane directions, but promote multidirectional twinning. Most recent studies rather focused on the impact of Sr on the nucleation of eutectic Si. In the commercial A356 alloy, phosphorus (P) normally exists as impurity. It reacts with Al in the liquid and produces a fine dispersion of aluminium phosphide (AlP) particles, which act as potent nuclei for eutectic Si. Dahle *et al.* [5] suggested that the potency of AlP particles to nucleate the Si phase is reduced by the competitive formation of Al_2Si_2Sr, which nucleates on AlP. In the numerical studies of Eiken *et al.* [6, 7], both aspects were considered and verified by 3D phase field (PF) simulations coupled with a thermodynamic database for the Al-Si-Sr-P system.

Macroscopic casting simulations incorporating solidification models are often applied to optimize process parameters and geometries of casting components. Commonly, Scheil-Gulliver approximations are employed in casting simulations to estimate the solidification path, i.e. the temperature dependent fraction of solid $f_s(T)$ and the latent heat release. However, the Scheil-Gulliver model fails to describe the effect of Sr on the nucleation and growth process of eutectic Si phase. This model leads to an inaccurate description of the solidification path, as it does not consider recalescence or growth undercooling of the eutectic.

In order to address this problem, a dedicated micro-macro coupled simulation approach is proposed here. In this approach, the thermomechanical finite element casting simulation is coupled with microstructure formation simulations based on a homoenthalphic method proposed by Böttger *et al.* [8]. The spatially resolved microstructure simulations were performed using a Calphad-based multicomponent multiphase-field (MMPF) model [9]. The dimensions of the representative volume element (RVE) has been selected based on the experimental observed average grain size. In the studied case, i.e. Sr-modified hypoeutectic Al-Si alloys, the interdendritic eutectic has a much finer microstructure, compared to primary fcc-Al dendrites. Therefore, the two-phase eutectic was not spatially resolved, but handled as an effective single phase in the MMPF simulation. The effect of Sr-modification was achieved by adjusting the nucleation model for eutectic Si phase, and by calibrating a growth parameter which characterizes the critical length scale of the eutectic microstructure. The MMPF simulation covers the physical complexity of the solidification process and provides an improved description of solidification path and latent heat release to the macroscopic casting simulation.

Moreover, to derive the effective mechanical properties of the mushy zone, a two-level homogenization scheme based on an asymptotic expansion of the involved periodic fields [10, 16] is adopted here. At the fine scale level, the fibrous eutectic morphology is homogenized based on a microstructure simulation on a smaller RVE that resolves the growth of the fine eutectic structure. Then, at the larger scale level, microstructures containing primary fcc-Al dendrite, effective eutectic and residual melt are homogenized with a mixed finite element discretization, which is suitable to model the melt incompressibility [10]. The proposed multiscale simulation approach was applied to a permanent mould casting using an axisymmetric bowl cast from A356 alloy for experimental validation.

2. Homoenthalpic approach for micro-macro coupling

In macroscopic casting simulations, the casting alloys are commonly treated as a liquid/solid coexisting system, which is characterized by the temperature dependent fraction solid $f_s(T)$. In practice, as it is more convenient to measure the specific heat at constant pressure than at constant volume, the state variable enthalpy is always used in the thermal analysis of solidification. Following Dantzig and Rappaz [11], the average form of the local energy balance in terms of specific enthalpy can be expressed as:

$$\frac{\partial\langle\rho h\rangle}{\partial t}+\boldsymbol{\nabla}\cdot\langle\rho h\mathbf{v}\rangle=\dot{\mathrm{Q}}+\langle\rho r\rangle\,, \tag{1}$$

in which ρ and h denote the density and specific enthalpy, respectively. $\mathbf{v}$ represents the velocity vector, $\dot{\mathrm{Q}}$ is the heat flux, and $\langle\rho r\rangle$ is a heat source term. Here, $\langle\bullet\rangle$ represents the volume average of a quantity in the two-phase system. By introducing the specific heat capacity c_p and the latent heat release L_f during the solidification, the average enthalpy of the mixture can be expressed as

$$\langle\rho h\rangle=\int_{T_0}^{T}\left\langle\rho\, c_\mathrm{p}(\tilde{T})\right\rangle\,\mathrm{d}\tilde{T}+\langle\rho\rangle\, L_\mathrm{f}\left[1\text{-}f_\mathrm{s}(\mathrm{T})\right] \tag{2}$$

with its time derivative calculated as

$$\frac{\partial\langle\rho\, h\rangle}{\partial t}=\left\langle\rho\, c_\mathrm{p}\right\rangle\frac{\partial T}{\partial t}\text{-}\langle\rho\rangle L_\mathrm{f}\frac{\partial f_\mathrm{s}}{\partial T}\frac{\partial T}{\partial t}. \tag{3}$$

In absence of external heat sources, i.e. $\langle\rho r\rangle$=0, substituting equation (3) into equation (1) leads to

$$\left(\left\langle\rho\, c_\mathrm{p}\right\rangle+\langle\rho\rangle L_\mathrm{f}\frac{\partial f_\mathrm{s}}{\partial T}\right)\frac{\partial T}{\partial t}+\boldsymbol{\nabla}\cdot\langle\rho\, h\,\mathbf{v}\rangle=\dot{\mathrm{Q}}\,. \tag{4}$$

In this coupling approach, the heat capacity, the latent heat release and the fraction solid are obtained by performing the Calphad-based MMPF microstructure simulation. Outcomes of the macroscopic process simulation, e.g. the local heat extraction rate $\dot{Q}$ and local temperature gradient, are applied as boundary conditions in microstructure simulations. In the MMPF simulation, the volume averaged enthalpy change in the current time step is calculated as

$$\mathrm{d}H^{t_n}=\frac{1}{V_c}\int_{V_c}\sum_{\alpha}\mathrm{d}\left(\phi_\alpha^{t_n}H_\alpha\left(T^{t_n}\right)\right)\mathrm{d}v\ , \tag{5}$$

where ϕ_α and H_α are the phase fraction and the molar enthalpy of phase α, respectively. The increment of volume averaged latent heat release $\mathrm{d}\bar{L}_f^{t_n}$ is then calculated based on the average heat capacity from the previous time step, i.e.,

$$\mathrm{d}\bar{L}_f^{t_n}=\mathrm{d}\bar{H}^{t_n}-\bar{C}_p^{t_{n-1}}\,\mathrm{d}T^{t_{n-1}}\quad\text{with}\quad\bar{C}_p^{t_{n-1}}=\frac{1}{V_c}\int_{V_c}\sum_{\alpha}\phi_\alpha^{t_{n-1}}\,C_{p,\alpha}\mathrm{d}v\,. \tag{6}$$

The volume and phase-specific enthalpy H_α and heat capacity $C_{p,\alpha}$ are read from the thermodynamic database of ThermoCalc®. The updated fraction solid, latent heat release and heat capacity in dependency of temperature can then be applied for improving the macroscopic process simulation.

3. Macroscopic casting simulation model

The proposed approach was applied to simulate the solidification process of a die casting component. The macroscopic casting simulation was performed by using the finite element (FE) software Abaqus. The model was built according to the experimental set-up presented in [12]. As illustrated in figure 1(a), the model mainly consists of an inner steel core, a steel mould, a sand core on the top and the axisymmetric bowl shaped casting component. The bowl component has an outer diameter of 155 mm and a wall thickness that gradually varies from 15 mm up to 30 mm. The insulation on bottom and the sand core on top of the bowl assured a radial flow of the heat flux. The steel mould was built up with three identical 120° segments, which include cooling channels and thermo-elements. For this reason, one third of the entire set-up was modelled for FE simulations. According to the casting experiment, the melt, i.e. the bowl region had an initial temperature of 720 ºC, while the mould temperature was set to 30 ºC.

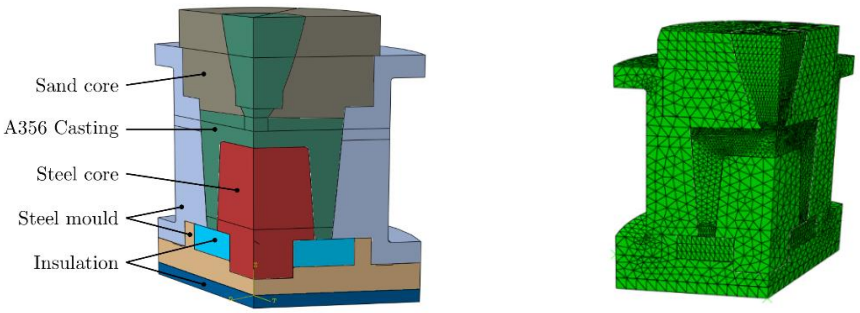

(a) (b)

Figure 1. (a) Construction of the experimental set-up; (b) Finite element mesh with temperature-displacement coupled 4-node linear tetrahedral elements.

The model is meshed with temperature-displacement coupled 4-node linear tetrahedral elements, see figure 1(b). As in casting simulations the thermal and mechanical solutions strongly interact, a fully coupled thermal-stress analysis is performed. The A356 component was modelled as thermo-elastoplastic material, while the mould and core parts are thermo-elastic materials. In order to model the phase transformation, a user specific subroutine was written to specify the internal heat generation due to the latent heat release along the solidification path according to equation (4). As the bowl component undergoes a volume shrinkage during the solidification process, air gap could be formed between the casting component and mould. For further precision of the simulation, the contact condition between

the bowl component and its surrounding mould was distinguished between fluid-solid and solid-solid surface contact. By modelling the solid-solid surface contact condition, the impact of the formed air gap on the heat transfer coefficient (HTC) was taken into account. In this case, the gap conduction model is written as a function of the local gap width and the local contact pressure [13].

In experiments, a commercial A356 with Sr-modification and grain refinement (TiB5) was applied for the casting. The grain refinement ensures equiaxial growth of fcc-Al dendrites over the entire casting component and a relatively homogenous grain size distribution. This behaviour allows the application of a uniform fraction solid $f_s(T)$ and enthalpy-temperature relations over the whole component in the casting simulation.

4. Microstructure simulation model

The phase formation sequence of unmodified A356 alloys during the solidification was firstly calculated via the thermodynamic computation based on Scheil-Gulliver model using the software ThermoCalc®. Here, the alloy system is defined by 92.7 wt% Al, 7 wt% Si and 0.3 wt% Mg. Further chemical elements normally contained in commercial A356 alloys, as Mn and Fe, are not considered. As shown in figure 2, the equilibrium eutectic temperature in the unmodified alloy under Scheil condition is 575.3 ºC.

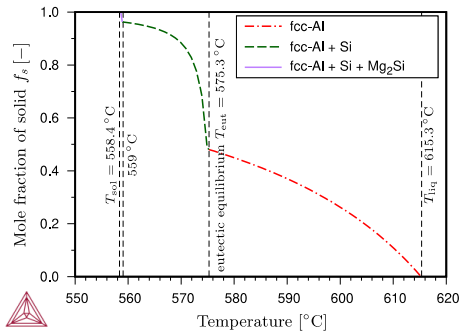

Figure 2. Scheil calculation for unmodified A356 alloy using ThermoCalc with database TCAL5.

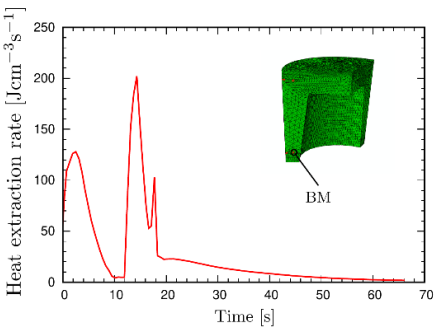

Figure 3. Heat extraction rate read from the casting simulation result on the bottom middle (BM) point of the bowl

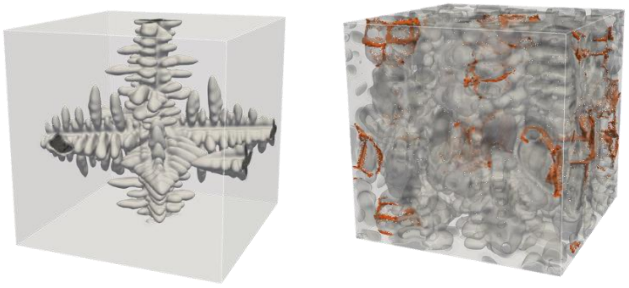

(a) (b)

Figure 4. Results of 3D microstructure simulation: (a) one single primary fcc-Al dendrite at t=0.8 s and T=599.4 °C; (b) primary fcc-Al and interdendritic eutectic (orange coloured) at t=10 s and T= 571.7 °C.

The microstructure simulations were performed using the software MICRESS®, which is based on the MMPF model specified in [9]. The Calphad-database are coupled via the TQ-interface. According to experimental observations, the simulation was performed on a 3D-domain with a size of 320 µm^3 and a grid resolution of 2 µm. The simulation started from 100% liquid at 615 ºC. As boundary condition, heat was extracted from the RVE according to the casting simulation results (see figure 3). The eutectic was treated as an effective single phase. Iterative micro-macro simulations were performed to obtain consistent enthalpy-temperature relation. As no additional temperature gradient exists, an equiaxed single fcc-Al dendrite growths at the beginning of the solidification, see figure 4(a). At higher solid fractions, interdendritic eutectic was formed between primary fcc-Al dendrites and residual melt, leading thus to a rather complex microstructure, see figure 4(b).

4.1. The impact of Sr on the eutectic solidification

The impact of Sr on the eutectic solidification was considered by applying appropriate nucleation and growth parameters for the effective eutectic phase. Specifically, the effect of Sr on the growth was simulated by calibrating a parameter which characterize the critical length scale of the eutectic morphology, whereas its effect on the nucleation of eutectic Si was realized by adjusting the number of initial nuclei for the eutectic phase.

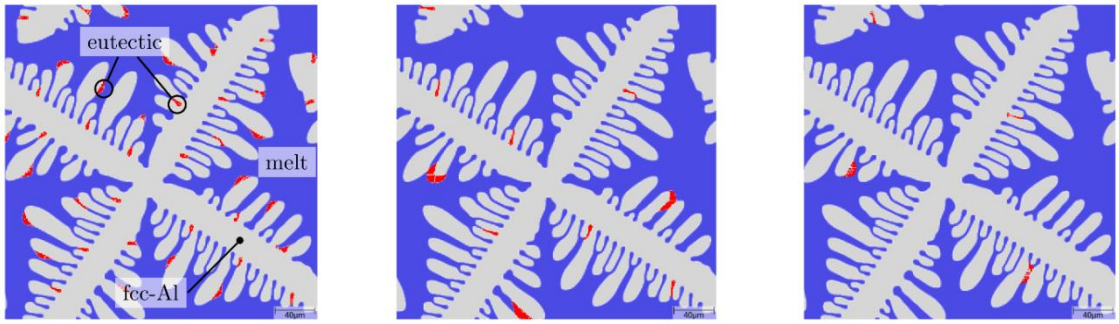

(a) (b) (c)

Figure 5. Distribution of eutectic Si nucleation sites (red coloured) at the beginning of eutectic solidification for different simulation scenarios (a) unmodified A356 alloy; (b) A356 with lower Sr content; (c) A356 with higher Sr content.

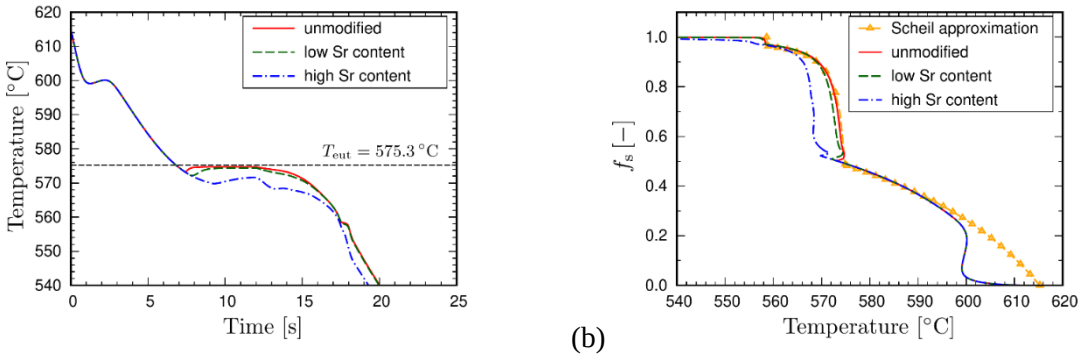

(a) (b)

Figure 6. Temperature evolutions (a) and fraction solid curve (b) of three different scenarios.

As shown in figure 5, three different scenarios have been simulated in 2D and compared. In scenario (a), i.e. unmodified A356 alloy, more potent nuclei for eutectic Si were distributed in the interdendritic region and lead to the growth of eutectic grains. In scenarios (b) and (c), modified A356 with different Sr contents were simulated. The higher the Sr content, the fewer Si nuclei appear in the simulation region. The effect of Sr-modification was fully embodied by the reduced eutectic growth temperature. As illustrated in figure 6(a), in the unmodified case the eutectic growth temperature is very close to the equilibrium temperature obtained by Scheil approximation, while by high Sr content it is nearly 5 °C lower. Additionally, recalescence has been observed in the primary solidification (fcc-Al). Consequently, the fraction solid curve differs to the Scheil approximation, see figure 6(b). The fraction solid curve obtained from the MMPF simulation was then transferred to the macroscopic casting simulation in order to take into account the effect of Sr-modification.

5. Coupled multiscale simulation results

The coupled multiscale simulation approach was performed in two iterative loops. It began with a FE casting simulation with the classical Scheil approximation. The obtained local heat extraction was then applied as boundary condition for the temperature calculation in the MMPF simulation based on the energy balance. In the second FE simulation, the new fraction solid curve and latent heat release obtained from the microstructure simulation was applied.

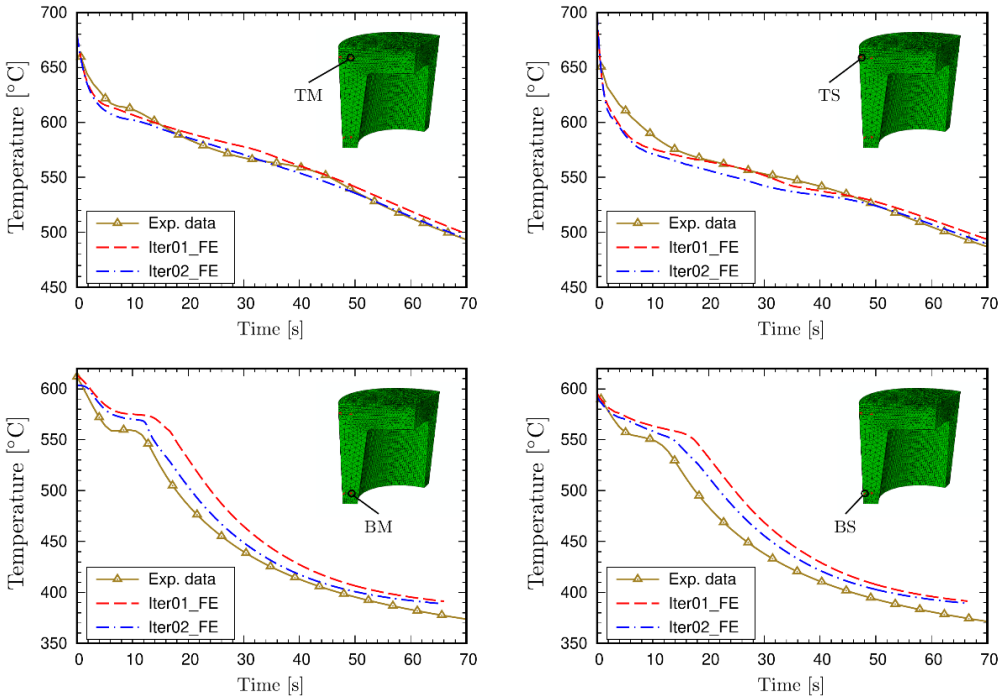

Figure 7. Temperature evolutions obtained by FE casting simulations on four experimentally observed locations, which are labelled as TM (top middle), TS (top surface), BM (bottom middle) and BS (bottom surface).

For validation, the simulated temperature evolutions in four different bowl locations have been compared with the experimental measurements in figure 7. It can be seen that, the FE simulation with the Scheil approximation (Iter01_FE) supplied good temperature predictions in locations TM and TS. However, on the bottom of the bowl (locations BM and BS) where the cooling rate is higher, the predicted temperature was significantly higher than in the experiment, especially at the later stage of solidification. By applying the fraction solid-temperature relationship and the latent heat release from the MMPF simulation in the second FE simulation (Iter02_FE), a better agreement between predicted and experimental temperatures was achieved. For further improvements of the FE simulation results, 3D MMPF simulations have to be performed for more accurate description of recalescence and the impact of Sr on the eutectic growth temperature.

6. Two-level homogenization of 3D A356 microstructures

As the experimental characterization of the mechanical behaviour of the mushy zone during Al alloy solidification is delicate, the locally performed 3D MMPF simulations were used to derive accurate effective elastic properties of the mush by applying a two-level homogenization scheme.

6.1. Homogenization of the coral-like structure of Si eutectic

As outlined in detail in [6, 7], the effect of Sr on the twinning of Si in eutectic was modelled on the finer scale implicitly by adopting an effective anisotropic surface mobility. From the converged 3D large scale simulation of the solidification of Sr modified A356, the temperature and concentration fields were locally extracted in the melt near primary dendrite arms. These local fields are applied as initial conditions on a fine discretized, small RVE at the lower scale. A single nucleation seed of Si was adopted in the 3D MMPF simulation of the eutectic formation. From this nucleus a complex, coral-like fibrous Si eutectic morphology grows around the primary fcc Al-dendrite during further solidification.

From this microstructure, four pure eutectic RVE's have been extracted (see figure 8, where two extracted RVE's are shown). Their Si content varies from 10.61% up to 15.35%, leading to a mean Si content of 12.90%.

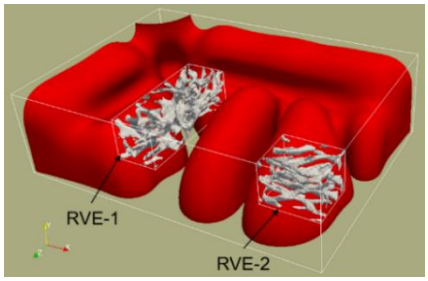

Figure 8. Extraction of RVE-1 and RVE-2 of pure eutectic near a fcc-Al dendrite.

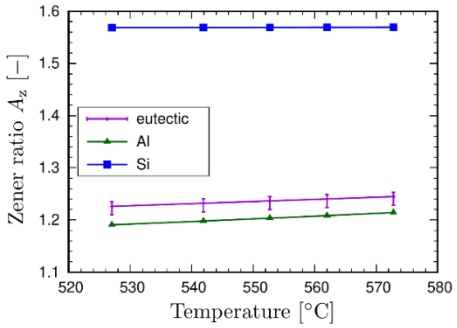

Figure 9. Temperature variation of the Zener ratio A_z and its scatter for effective eutectic, pure single crystal Al and Si.

The temperature dependent elastic properties of the single crystals Al and Si were taken from [14] and [15], respectively. The homogenization of the four RVE's was performed not only to determine the mean elastic constants of the eutectic but also to quantify the influence of the scatter of the Si content on their values. *The effective eutectic is cubic* and presents a noticeable effective Zener anisotropy coefficient A_z, which increases slightly with the temperature, as shown in figure 9. Note that the Si content scatter affects mainly the effective shear modulus C_{44}; whereas the effective elastic constant C_{11} is nearly unaffected.

6.2. Homogenization of equiaxed dendritic 3D microstructures

At selected time steps of the 3D MMPF simulation of local A356 solidification, the actual microstructure was transferred to the homogenization tool HOMAT to calculate the effective mechanical properties. The implemented homogenization scheme is based on the asymptotic expansion method outlined in [16]. Effective thermal conductivities of the mushy zone have already been presented in [18].

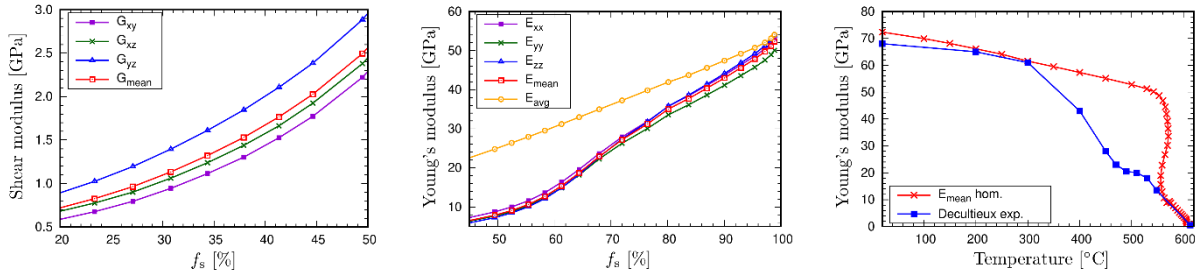

(a) (b) (c)

Figure 10. Variation of the effective shear modules (a) Young modules (b) with the solid fraction. Variation of the homogenized and experimental Young modules with the temperature (c).

The thermoelastic homogenization of the different microstructures provided amongst others the results outlined in figure 10. The variation of the effective shear modules with f_s for the primary solidified Al dendrites shows a pronounced orthotropy: $G_{yz}>G_{xz}>G_{xy}$. The in-plane shear modulus G_{xy} presents the lowest stiffness. This homogenization is performed for f_s above shear coherency ($f_s \approx 0.22$) [17], at which the much develops first shear resistant due to dendrites entanglement. Figure 10(b) displays the variation of the directional Young modules, their mean value and the volume averaged Young modulus with f_s above the estimated traction coherency $f_{s,tr} \approx 0.48$. Obviously, Si induces a stronger increase of the effective Young modules during the eutectic formation than during the pure Al dendrite formation. Due to the calculation of correction terms, the 1st order homogenization scheme [16] improves the volume averaging prediction mainly at the end of the primary solidification, where the solid-liquid interfaces are at the largest. Eventually, figure 10(c) shows the temperature evolutions of the mean effective Young's modulus and of an experimentally measured Young's modulus from uniaxial tensile tests [19] over the complete cooling path. Due to recalescence and undercooling effects,

the $E(T)$ curve is not unique in the mushy region. Therefore, the more accurate $E(f_s)$ has to be derived in the mushy region. A large discrepancy between experimental and predicted Young's modulus curves is observed at higher temperatures ($T > 300°C$). It can be explained by the fact that in the experiment the viscous component, present always at higher temperatures, cannot be separated from the pure elastic one, as achieved in the homogenization, where only pure elastic Young's moduli were derived.

7. Conclusions

The present work confirmed that thermomechanical casting simulations based on fraction solid curves derived under Scheil-Gulliver assumptions are not able to provide a predictive simulation result in the case of Sr-modified Al-Si alloys. In the proposed multiscale simulation approach, the multicomponent multi-phase field based microstructure simulation effectively depict the effect of Sr-modification on the nucleation and growth of eutectic Si phase. The more realistic thermodynamic description of the solidification process provided by the MMPF simulations significantly improved the temperature prediction, especially in regions with high cooling rate. Effective mechanical material properties were derived based on a two-level homogenization approach. The results show that the complex fibrous morphology of the multiphase eutectic material exhibit an effective cubic behaviour. Moreover, it was found that the effective mechanical mushy zone properties have to be expressed as a function of fraction solid rather than as a function of temperature, as the temperature dependence is non-unique. An interesting task will be to study the impact of the homogenized Young's moduli on the local stress-strain state in future thermomechanical casting simulations. Virtual tests will be performed on the predicted microstructures in order to derive the effective viscoplastic flow behaviour of the A356 mush and to identify unknown parameters of the thermo-elasto-plastic constitutive laws, developed in ref. [17] for the coherent and non-coherent mushy zones.

Acknowledgments

The authors would like to acknowledge support from the German Research Foundation (DFG) in the framework of the Collaborative Research Centre SFB1120-236616214 "Precision Melt Engineering".

References

[1] Sigworth G K 2008 *Int. J. Met.* **2** 41
[2] Timpel M *et al.* 2012 *Acta Mater.* **60** 3920–28
[3] Lasko G, Apel M, Carré A, Weber U and Schmauder S 2012 *Adv. Eng. Mater.* **14** 236–247
[4] Lu S Z and Hellawell A 1987 *Metall. Trans. A* **18** 1721–33
[5] Dahle A K, Nogita K, McDonald S D, Dinnis C and Lu L 2005 *Mater. Sci. Eng. A* **413** 243–8
[6] Eiken J, Apel M, Liang S M and Schmid-Fetzer R 2015 *Acta Mater.* **98** 152–163
[7] Eiken J and Apel M 2015 *IOP Conf. Ser. Mater. Sci. Eng.* **84** 012084
[8] Böttger B, Eiken J and Apel M 2009 *J. Comput. Phys.* **228** 6784–95
[9] Eiken J, Böttger B and Steinbach I 2006 *Phys. Rev. E-Stat. Nonlinear, Soft Matter Phys.* **73** 1–9
[10] Laschet G, Nokhostin H, Koch C, Meunier M and Hopmann C 2020 *Mech. of Mat.* **140** 103225
[11] Dantzig J A and Rappaz M 2009 *Solidification* (EPFL Press)
[12] Wolff N, Pustal B, Vossel T, Laschet G and Bührig-Polaczek A 2017 *Materwiss. Werksttech.* **48** 1235–40
[13] Laschet G, Jakumeit J and Benke S 2004 *Zeitschrift für Met.* **95** 1087–96
[14] Sutton P M 1953 *Phys. Rev.* **91** 816–21
[15] Masolin A, Bouchard P O, Martini R and Bernacki M 2013 *J. Mater. Sci.* **48** 979–988
[16] Laschet G and Apel M 2010 *Steel Res. Int.* **81** 637–643
[17] Laschet G and Behnken H 2019 *IOP Conf. Ser. Mater. Sci. Engng*. **529** 012083.
[18] Laschet G, Vossel T, Wolff N, Apel M and Bührig-Polaczek A 2017 *SP17 Proc. 6th Decenn. Int. Conf. Solidif. Proceeding (Old Windsor)* ed Fan Z (Middlesex, UK: BCAST) pp 576–80
[19] Decultieux F 1996 *PhD thesis* (CEMEF, Paris Tech.)